

# Soybean $\beta$ -Conglycinin Nanoparticles for delivery of hydrophobic nutraceuticals

Yonatan Levinson · Gal Israeli-Lev · Yoav D. Livney

Received: 11 February 2014 / Accepted: 5 May 2014 / Published online: 31 May 2014  
© Springer Science+Business Media New York 2014

**Abstract** We report the formation of nanoparticles using soybean  $\beta$ -conglycinin ( $\beta$ -CG), a globular storage protein, to encapsulate vitamin D (VD), as a model hydrophobic nutraceutical for food fortification applications. VD- $\beta$ -CG nanoparticles were formed in phosphate buffer, at both pH 6.8 and pH 2.5, by drop-wise addition of ethanol-dissolved VD to  $\beta$ -CG solution at room temperature, while vortexing. Turbidity measurements of the nanoparticle solutions showed optical clarity compared to VD in phosphate buffer which, in the absence of  $\beta$ -CG, formed suspensions whose turbidity increased almost linearly with vitamin concentration. Dynamic light scattering measurements revealed that while VD in buffer formed particles with a mean diameter of ~600 nm, the VD- $\beta$ -CG nanoparticles had mean diameters in the 50–400 nm range.  $\beta$ -CG also protected VD from several forms of degradation: After exposure to 70 °C for 30 s at pH 2.5, VD was reduced by 75 % whereas the VD- $\beta$ -CG nanoparticles lost only 2.5 % of their vitamin content. At the end of a three week shelf life test, nanoparticles retained 70 % and 90 % of their vitamin content at pH 6.8 and 2.5, respectively, whereas the protein-free controls retained only about 13–22 % (with no significant difference between retention at these two pH values). After two hours of simulated gastric digestion, the nanoparticles retained over 90 % of their vitamin content, whereas protein-free controls retained only ~50 % of their vitamin content. These results highlight the potential of  $\beta$ -CG as a nanoencapsulation agent for hydrophobic nutraceuticals for enrichment of food and beverages, including clear ones.

**Keywords**  $\beta$ -Conglycinin · Vitamin D<sub>3</sub> · Nanoparticles · Delivery

## Introduction

Among the materials used for encapsulating drugs and nutraceuticals, amphiphilic block copolymers are particularly well suited for entrapping lipophilic compounds. Amphiphilic block copolymers contain both hydrophilic and hydrophobic monomers grouped in contiguous patches, and can therefore self-assemble into particles with hydrophilic external shells and hydrophobic cores, into which lipophilic molecules can be loaded [1,2]. Certain proteins possess similar properties, as they contain both polar and non-polar amino acids grouped in blocks, the latter forming hydrophobic regions or pockets in the protein's structure. These hydrophobic regions can act as binding sites for lipophilic compounds or, alternatively, multiple protein molecules can self-assemble into nano-sized micelles or clusters whose hydrophobic cores contain the compounds [2,3]. Lipophilic compounds can thus be solubilized in an aqueous environment, and also protected from environmental factors such as heat, UV light, and oxidation. Furthermore, if ingested, proteins are broken down as they pass through the digestive system, releasing their nutraceutical cargo and facilitating its absorption, making this type of encapsulation ideal for nutraceutical fortification and delivery. Examples of such systems include casein micelles (model compounds used: vitamin D (VD) [4], curcumin [5]);  $\beta$ -lactoglobulin (DHA [6], VD [7], EGCG [8], caffeine [9], and folic acid [10]); and bovine serum albumin (tetracycline [11]). While milk proteins have excellent properties for delivery applications [12], they cannot be used in certain products, such as vegan and Kosher-PARVE foods. Hence, we sought a plant protein with similar properties, and soybean proteins

Y. Levinson · G. Israeli-Lev · Y. D. Livney (✉)  
Department of Biotechnology and Food Engineering, Technion,  
Haifa 3200000, Israel  
e-mail: livney@technion.ac.il

have long been known as plant-based substitutes for milk proteins for various food applications.

Soy Protein Isolate (SPI) is a storage-protein rich powder made from defatted soybeans. It is primarily comprised of glycinin (the 11 s fraction, ~52 % of the protein) and  $\beta$ -Conglycinin ( $\beta$ -CG) (the 7 s fraction, ~35 % of the protein) [13].  $\beta$ -CG is a water soluble heterotrimer containing three types of subunits:  $\alpha$ ,  $\alpha'$  (whose sequences are very similar) and  $\beta$ . Six isomers, containing various combinations of these subunits, are observed in nature [14,15]. Subunits  $\alpha$ ,  $\alpha'$  and  $\beta$  have molecular weights of 67, 71 and 50 kDa, respectively [16], and the calculated average molecular weight of the six naturally found isomers is ~190 kDa. The  $\alpha$  and  $\alpha'$  subunits each contain a relatively hydrophobic core region, and a hydrophilic extension region, while the  $\beta$  subunit contains only the hydrophobic core region; in addition, all subunits are glycosylated [16]. SPI has been used for encapsulation of fish oil [17], and curcumin [18,19]. SPI-carboxymethyl chitosan nanoparticles have recently been used to encapsulate VD [20]. However, nanoparticles consisting only of  $\beta$ -CG have not been reported. Because  $\beta$ -CG is the more amphiphilic component of SPI, and has better emulsification properties than glycinin [21–23], we have chosen to focus on its potential to serve as a delivery system for hydrophobic nutraceuticals, using VD as a model.

VD deficiency and insufficiency, defined as serum 25-hydroxyvitamin D levels lower than 20 ng/ml or between 21 and 29 ng/ml, respectively, are widespread conditions that affect an estimated one billion people globally [24]. Although this condition has historically been associated with calcium related diseases such as rickets, osteoporosis and osteopenia, new data suggest that maintaining proper levels of VD helps preventing a host of illnesses, ranging from muscle weakness [25], cancer (colorectal [26], and prostate [27]), diabetes [28] and cardiovascular diseases [29]. VD is important for regulation of immune functions and for decreasing the risk of autoimmune diseases [28]. For these reasons, there is a high demand for VD dietary supplements, in the form of vitamin D<sub>2</sub> or D<sub>3</sub> (VD<sub>2</sub> and VD<sub>3</sub>, respectively), the latter being the body's natural precursor to 25-hydroxyvitamin D, the circulating storage form of VD. Of the two supplements, VD<sub>3</sub> has been shown to be more efficient in increasing serum levels of 25-hydroxyvitamin D [30]. Over-the-counter supplements in pill or liquid form are available, but due to the widespread nature of VD deficiency, there is a growing demand for fortified food and beverage products, to reach the general population [31]. Because of this demand, and because of VD<sub>3</sub>'s highly hydrophobic nature (calculated octanol/water logP=10.24 [32]), we have chosen it as a model compound to test the encapsulation potential of  $\beta$ -CG.

In this study, VD<sub>3</sub> was added to  $\beta$ -CG solutions to form VD<sub>3</sub>- $\beta$ -CG complexes. These were characterized by measuring sample turbidity and particle size distribution, and by

observing nanoparticle morphology using cryo-TEM microscopy. The protective effect of  $\beta$ -CG on the bound VD<sub>3</sub> was measured by subjecting samples to heat treatment, shelf life conditions, and simulated gastric digestion, then quantifying VD<sub>3</sub> content by solvent extraction and reversed phase liquid chromatography (RP-HPLC).

## Materials and Methods

### Materials

Powdered  $\beta$ -CG (>95 % purity) was generously provided by Solbar (Ashdod, Israel). Cholecalciferol/VD<sub>3</sub> (C1357), Bradford Reagent (B6916), porcine pepsin (0.86 mg protein/mg solid), and HPLC grade  $\geq$ 99.9 % methanol (34,860) and acetonitrile (34,998) were obtained from Sigma-Aldrich (Rehovot, Israel).

### Methods

#### *Preparation of VD<sub>3</sub>- $\beta$ -CG nanoparticles*

One mg/ml  $\beta$ -CG solution was prepared as follows: 200 mg of dry  $\beta$ -CG powder were dissolved in 40 ml of either 30 mM pH 6.8 phosphate buffer (PB) or 25 mM pH 2.5 PB, each containing 0.02 % sodium azide as preservative, and set on a rotating mixer overnight at room temperature to obtain maximal protein dissolution. To remove undissolved solids, the protein solution was divided into 2 ml Eppendorf tubes, centrifuged at 1,500 xg for 15 min, and the supernatant was filtered through 0.45  $\mu$ m filters. Final protein concentration was quantified by the Bradford assay, using a reference concentration of bovine serum albumin (BSA). BSA was prepared both at pH 6.8 and 2.5, and separate assays were conducted to quantify  $\beta$ -CG prepared at different pH levels.

Nanoparticles were prepared by dissolving dry VD<sub>3</sub> in pure ethanol, and adding the ethanol stock solution dropwise into a glass vial or test tube containing 1 mg/ml  $\beta$ -CG solution, while vortexing. The final ethanol concentration was 2 %. The mixture was then put on an orbital shaker for 2 h for equilibration.

#### *Turbidity and Size Distribution*

Fresh VD<sub>3</sub> stock solution was prepared at 10 mg/ml in pure ethanol and titrated to 5, 3.75, 2.5, 1.25 and 0.625 mg/ml. Using these concentrations, nanoparticles were prepared, as described above, at a constant  $\beta$ -CG concentration of 1 mg/ml. The final VD<sub>3</sub> concentrations were 100, 75, 50, 25 and 12.5  $\mu$ g/ml. Samples were loaded into a quartz cuvette and absorbance at 600 nm was measured using an Ultrospec 3,000 UV/Visible spectrophotometer (GE Healthcare,

Waukesha, WI, USA). Size distribution was measured by Dynamic Light Scattering (DLS) using a Nicomp™ 380 particle size/zeta potential analyzer (PSS, Santa Barbara CA, USA) at 23 °C. Particle size distributions were analyzed using the Nicomp™ volume-weighted distribution analysis.

Weighted average particle diameter is defined in Eq. 1,

$$\text{Weighted average particle diameter} = \sum_i^n d_i \varphi_i \quad (1)$$

where  $n$  is the number of separate peaks observed in a sample (typically between 1 and 3), and  $d_i$  and  $\varphi_i$  are the mean diameter (nm) and the (dimensionless) volume fraction of the  $i^{\text{th}}$  peak, respectively.

### 2.2.3 UV Absorbance Spectra

0.5 mg/ml  $\beta$ -CG was prepared with 25  $\mu\text{g/ml}$   $\text{VD}_3$  ( $\beta$ -CG- $\text{VD}_3$  M ratio 25:1) in PB pH 6.8, at 2 % ethanol, as described above, and its absorbance spectrum was measured using an Ultrospec 3,000 UV/Visible spectrophotometer. Absorbance spectrum of 0.5 mg/ml  $\beta$ -CG alone, and that of 25  $\mu\text{g/ml}$   $\text{VD}_3$  with 2 % ethanol, were also measured as controls. The absorbance spectrum of PB was subtracted from all sample spectra.

### Cryo-TEM Microscopy

For Cryo-TEM imaging, 1 ml samples of  $\beta$ -CG solution (1 mg/ml, pH 6.8) were prepared both alone and with  $\text{VD}_3$  added via the technique described above, with a final  $\text{VD}_3$  concentration of 50  $\mu\text{g/ml}$ , as well as  $\text{VD}_3$  in PB pH 6.8 at 20  $\mu\text{g/ml}$ . The specimens were prepared as thin liquid films (10–500 nm thick), on perforated polymer/carbon films in a controlled-environment vitrification system at  $25 \pm 0.01$  °C and 95–99 % relative humidity, and then quench-frozen in liquid ethane at its freezing point (–183 °C). This process is designed to prevent water crystallization during thermal fixation. In this manner, component segregation and rearrangement are mostly prevented, and the original fluid nanostructure is preserved. The technique and apparatus were described in detail previously [33]. Briefly the vitrified samples were then stored under liquid nitrogen (–196 °C), transferred to a Gatan 626 cooling holder via its “work station”, and observed in a Philips CM120 microscope at about –175 °C. Images were recorded at a 120 kV acceleration voltage, in a low-dose mode, to minimize electron-beam radiation damage. Gatan Multi Scan 791 cooled CCD camera was used to acquire the images, with the Digital Micrograph 3.1 software package.

### Quantification of $\text{VD}_3$ using RP-HPLC

To observe changes in the  $\text{VD}_3$  content of the nanoparticles following heat treatment, simulated gastric digestion and over the course of a simulated shelf life experiment,  $\text{VD}_3$  was extracted and quantified using the method described by Haham et al. [34], with slight modifications. All aqueous  $\text{VD}_3$ -containing samples were prepared in 1 ml volumes, in glass tubes. Three ml of 2:1 chloroform:methanol were added, and the mixture was vortexed for 20 s. Two ml of chloroform were then added, and the mixture vortexed for 1 min. The tubes were then centrifuged at 1,500  $\times g$  and 4 °C for 10 min, resulting in an organic layer of ~4 ml, from which 3 ml were drawn using a glass syringe, and transferred to a 20 ml glass vial. The vials were dried under mild  $\text{N}_2$  flow for 90 min at room temperature, in a fume hood.

The drying was followed by quantification using reverse-phase HPLC (RP-HPLC). 1.5 ml of RP-HPLC mobile phase (80 % acetonitrile, 20 % methanol, in accordance with the AOAC protocol [35]) were added to the dried samples, and allowed 15 min to equilibrate. Samples were run on an HP Agilent 1,100 HPLC system equipped with a diode array detector (DAD), and a 4.8 $\times$ 250 mm Vytac™ C-18 column. Injected sample volume was 20  $\mu\text{l}$ . An isocratic elution at a flow rate of 1.3 ml/min was used. Data analysis was conducted using the ChemStation software package (Hewlett-Packard, Wilmington, DE). In the mobile phase,  $\text{VD}_3$  has a local UV absorption maximum at 267 nm, which was used for  $\text{VD}_3$  quantification. At our flow rate of 1.3 ml/min, a peak eluted at a retention time of approximately 8.5 min. This peak was confirmed to be  $\text{VD}_3$  by observing its UV absorption spectrum, as recorded by the DAD.

$\text{VD}_3$  concentration in the mobile phase was quantified by integrating peak area (mAU\*min). To build a reference curve, solid  $\text{VD}_3$  was dissolved directly into the mobile phase at 50  $\mu\text{g/ml}$ , and diluted serially down to 0.6  $\mu\text{g/ml}$ . These solutions were run using the same RP-HPLC method, and the integrated peak area was plotted as a function of concentration and fit using simple linear regression. Dilution and extraction efficiency factors were determined and taken into account in calculating the original sample  $\text{VD}_3$  concentration.

### Thermal Degradation and Simulated Shelf Life

To better simulate real conditions,  $\beta$ -CG was freshly prepared in PB pH 6.8 and pH 2.5 without sodium azide. The following protocol was carried out twice, once at each pH: Twenty-one 1 ml samples of  $\text{VD}_3$ - $\beta$ -CG nanoparticles were prepared in glass tubes as described above, with a final  $\text{VD}_3$  concentration of 50  $\mu\text{g/ml}$  and a  $\beta$ -CG concentration of 1 mg/ml ( $\text{VD}_3$ : $\beta$ -CG molar ratio of 25:1). Twenty-one 1 ml  $\text{VD}_3$  samples with no  $\beta$ -CG were also prepared. Three tubes containing  $\text{VD}_3$ - $\beta$ -CG and three tubes containing unprotected  $\text{VD}_3$  were set aside

as controls and quantified via RP-HPLC. The remaining tubes were covered with Parafilm<sup>TM</sup> and subjected to a high-temperature short-time (HTST) treatment of 30 s at 70 °C, conducted in a hot water bath. A reference test tube containing a thermometer showed that approximately 1 min, 20 s were required to heat the samples from 23 to 70 °C, at which point they were held for an additional 30 s, and then immediately chilled on ice.

Immediately following heat treatment, three samples of both unprotected VD<sub>3</sub> and VD<sub>3</sub>-β-CG nanoparticles were extracted and quantified, with the results labeled as Day 0 of the simulated shelf life test. The remaining 30 samples were stored at room temperature, and loosely covered with aluminum foil to protect them from light, but allow oxygen exposure to obtain a stress test. On five different days over the course of a three week period, three samples of both unprotected VD<sub>3</sub> and VD<sub>3</sub>-β-CG nanoparticles were removed, and their VD<sub>3</sub> content measured using the RP-HPLC method described above. For each sample, preparation, heat treatment, and extraction all were performed in the same tube to eliminate transfer losses.

### Simulated Gastric Digestion

Because previous studies have indicated that β-CG is relatively resistant to pepsin proteolysis [36], we incubated samples of 1 mg/ml β-CG with different pepsin concentrations for 2 h at 37 °C to determine the protein:pepsin ratio which would completely digest the protein. The protein:pepsin w/w ratios ranged from 1,000:1 to 5:1. Sodium dodecyl sulfate-polyacrylamide gel electrophoresis (SDS-PAGE) indicated that, although the β subunit of β-CG displayed partial resistance against digestion at all protein:pepsin ratios, the alpha subunits were completely digested at a protein:pepsin ratio of 50:1 (results not shown). This ratio was, therefore, chosen to simulate gastric digestion.

For the simulation itself, 0.21 mg/ml pepsin stock solutions in 10 mM HCl were freshly prepared. VD<sub>3</sub> suspensions and VD<sub>3</sub>-β-CG nanoparticles were prepared in 1 ml samples in glass tubes, as described in the previous section. Thirty μl of 1 M HCl were added to lower the pH to 2.2. 130 μl were then removed from the samples, leaving 900 μl remaining. 100 μl of pepsin stock solution were then added to the sample, to achieve a final protein:pepsin ratio of 50:1. The sample tubes were incubated at 37 °C on an orbital shaker for 30, 60, 90 or 120 min, and then quenched with 30 μl of 1 M NaOH, adjusting the pH to 7 to inactivate the pepsin. Control samples received 100 μl of 10 mM HCl instead of pepsin, and were quenched immediately. The VD<sub>3</sub> content of the samples was analyzed using RP-HPLC as described above. All samples were prepared in duplicates.

### Statistical analysis

Data points represent the average of a set of replicates. Error bars represent the standard error (i.e. the std. deviation of the replicates divided by the square root of the number of replicates). For the heat treatment experiment, a two-sided *T*-test, assuming equal variance, was used to determine whether β-CG conferred a significant degree of protection to VD<sub>3</sub>, at a significance level of  $\alpha=0.05$ . The shelf life test was analyzed using OriginLab<sup>TM</sup> software (Version 8).

## Results and Discussion

### Prevention of VD<sub>3</sub> turbidity by β-CG

Turbidity is the result of suspended particles scattering visible light. It is usually quantified spectroscopically by measuring the absorbance of light in the visible range (600 nm), and subtracting the absorbance of a particle-free control solution. When added dropwise to pH 6.8 phosphate buffer, VD<sub>3</sub> formed cloudy suspensions whose turbidity increased almost linearly with VD<sub>3</sub> concentration (Fig. 1a). When added to a 1 mg/ml β-CG solution, however, the solution remained transparent. This clarification effect is shown in Fig. 2, which shows samples prepared at a final VD<sub>3</sub> concentration of 100 μg/ml. The effect was less readily observed at pH 2.5 due to the fact that VD<sub>3</sub> tended to aggregate into flakes and separate from the solution rather than form a turbid suspension, as it does at pH 6.8. Still, the absorbance of VD<sub>3</sub> in pH 2.5 PB was higher than in the β-CG solution (Fig. 1b).

### Particle Size Distribution

Figure 3a shows particle size distribution for VD<sub>3</sub> (50 μg/ml), β-CG (1 mg/ml) and VD<sub>3</sub>-β-CG (50 μg/ml, 1 mg/ml) at pH 6.8. Unencapsulated VD<sub>3</sub> had a monomodal distribution at all measured concentrations, and at both pH levels, with mean diameters of ~600–700 nm between 25 and 100 μg/ml at pH 6.8 (Fig. 3b) and 2,000–4,000 nm at pH 2.5 (Fig. 3c). This self-aggregation of VD<sub>3</sub> in water (also observed in a previous study from our group [34]) has been studied in depth by Meredith et al. [37], who found aggregates with a cylindrical micelle-like organization and an Rg of 530 nm (slightly larger than the sizes obtained here). This apparently results from the somewhat amphiphilic structure of VD<sub>3</sub>, as it has a hydroxyl group at one end while most of its structure is a hydrophobic steroid. Compared to the turbidity data, we see that, at pH 6.8 and above 25 μg/ml, the particle size remained constant, but since the concentration of particles increased, more light was scattered and the absorbance increased. The fact that, at pH 2.5, there were relatively large particles observed despite relatively low sample turbidity (Fig. 1b) can be



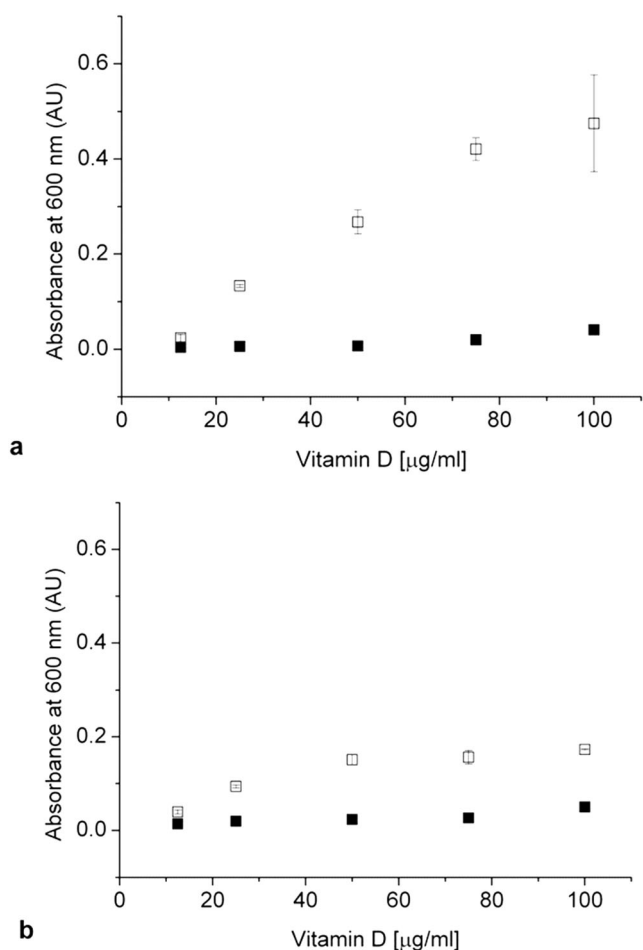


**Fig. 1** Turbidity of  $\text{VD}_3$  in PB (open) vs.  $\text{VD}_3$  in  $\beta\text{-CG}$  (closed) at pH 6.8 (a) and pH 2.5 (b)

explained by the fact that much of the  $\text{VD}_3$  simply precipitated out of solution, leaving behind a mostly clear liquid. This also explains the apparent decrease in mean particle size when concentration increased from 75 to 100  $\mu\text{g/ml}$  (Fig. 3c), due to precipitation of the large aggregates.

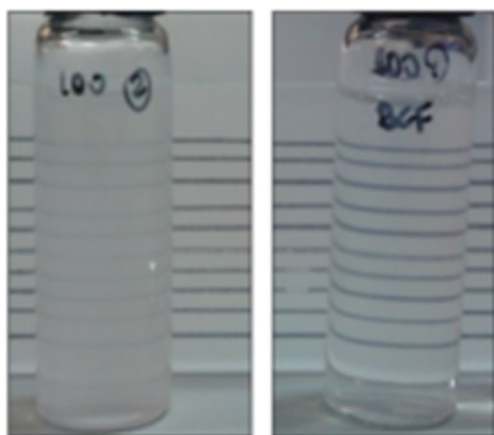


**Fig. 2** 100  $\mu\text{g/ml}$   $\text{VD}_3$  mixed into 1 mg/ml  $\beta\text{-CG}$  (right) and suspended in PB (left), both at pH 6.8

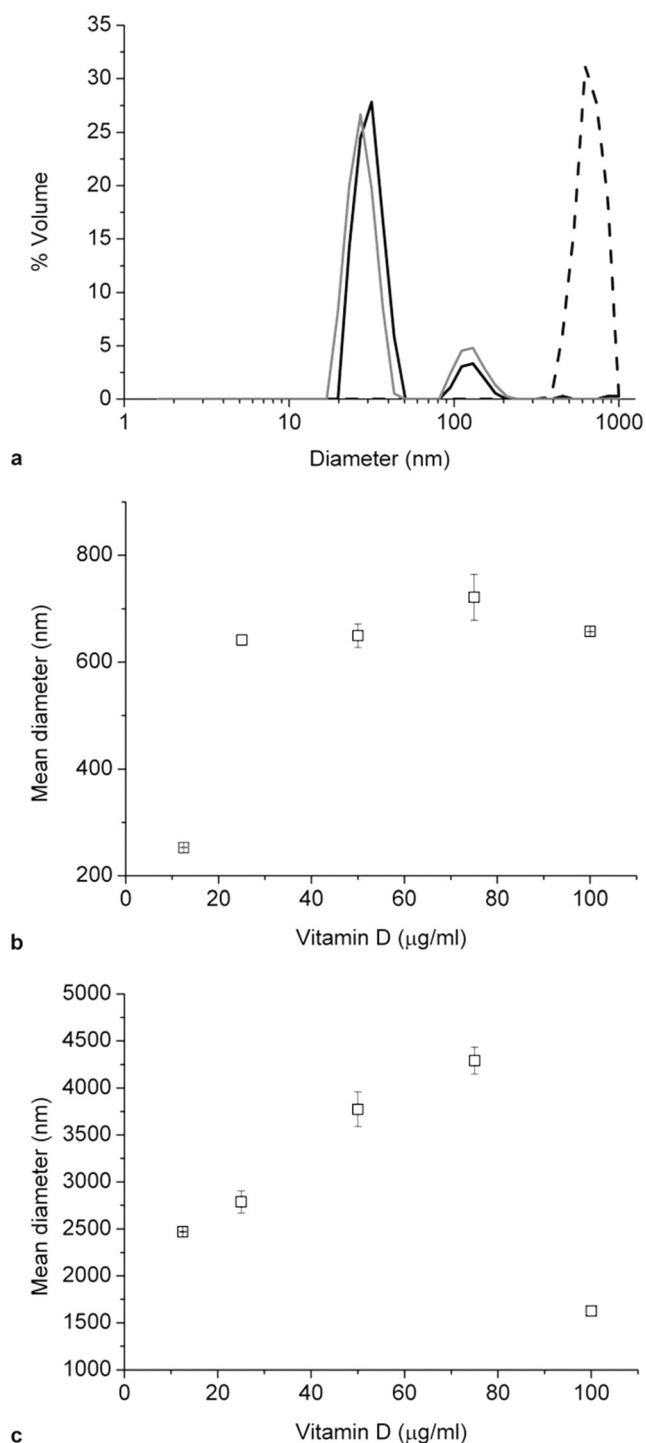


**Fig. 3** a) Particle size distribution of 50  $\mu\text{g/ml}$   $\text{VD}_3$  in pH 6.8 PB (dashed), 1 mg/ml  $\beta\text{-CG}$  (black), and  $\text{VD}_3\text{-}\beta\text{-CG}$  complex (gray), b) Mean particle diameter of  $\text{VD}_3$  at pH 6.8 c) Mean particle diameter of  $\text{VD}_3$  at pH 2.5

In contrast to unencapsulated  $\text{VD}_3$ , solutions of 1 mg/ml  $\beta\text{-CG}$  displayed a bimodal particle size distribution, with one population distributed about a mean diameter of 27 nm, accounting for ~90 % of total particles volume, and a second population distributed about a mean diameter of 120 nm,

accounting for the remaining 10 % (Fig. 3a). This distribution was observed at both pH 6.8 and pH 2.5. VD<sub>3</sub>- $\beta$ -CG samples had a similar bimodal distribution (Fig. 3a), with a 31 nm peak accounting for 90 % of the volume and a 120 nm peak accounting for 10 %.

To analyze how increasing VD<sub>3</sub> concentrations affected VD<sub>3</sub>- $\beta$ -CG particle size, we grouped all particles into two bins: small (0–50 nm) and large (>50 nm). We then plotted the volume fraction in each bin across all VD<sub>3</sub> concentrations, and at both pH levels (Fig. 4). At pH 6.8, the 90 % small, 10 % large particle distribution at 0 and 12.5  $\mu$ g/ml VD<sub>3</sub> shifted to 86 % small, 14 % large between 25–75  $\mu$ g/ml, and 70 % small, 30 % large at 100  $\mu$ g/ml VD<sub>3</sub> (Fig. 4a). At pH 2.5, we observed a similar shift, to 82–88 % small, 18–12 % large particles at 12.5–75  $\mu$ g/ml VD<sub>3</sub>, and 73 % small, 27 % large particles at 100  $\mu$ g/ml. Fig. 4 also shows the weighted average particle diameter at each concentration.

It is likely that the small particles observed are soluble  $\beta$ -CG monomers. In an X-ray crystallography study [38], a recombinant  $\beta\beta\beta$  homotrimer of  $\beta$ -CG was found to have an external diameter of 10 nm. The majority of native  $\beta$ -CG monomers, however, are larger, since they contain  $\alpha$  and  $\alpha'$  subunits, whose hydrophilic extension regions are not present in the  $\beta\beta\beta$  homotrimer, but would add to the monomer diameter in native  $\beta$ -CG.

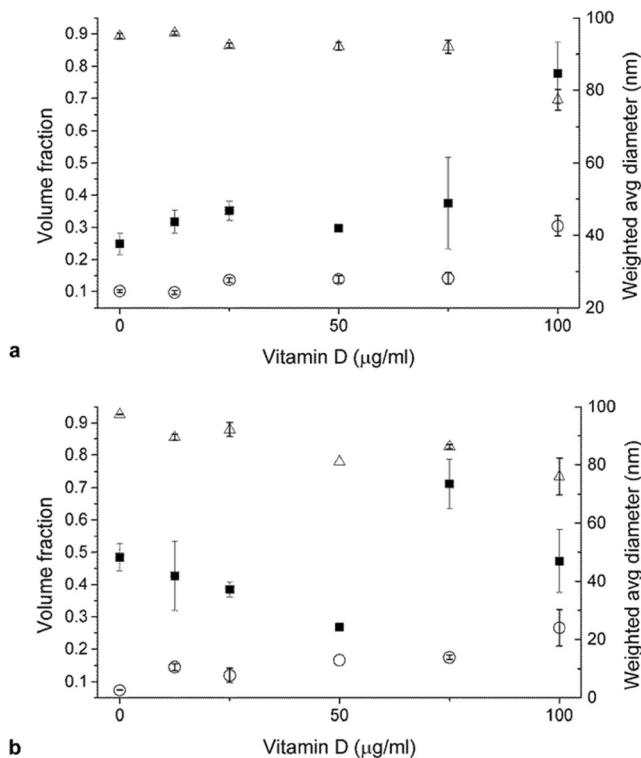


**Fig. 4** VD<sub>3</sub>- $\beta$ -CG particle size distribution characteristics at pH 6.8 (a), and pH 2.5 (b). The empty symbols represent the volume fraction (left axis) of the smaller, 0–50 nm particles (triangles) compared to that of the larger, 50–400 nm particles (circles). The full squares represent the volume-weighted average particle diameter (right axis)

The large particles, on the other hand, could either be  $\beta$ -CG monomers that spontaneously self-assembled, or heat-induced aggregates that were formed during the drying of the  $\beta$ -CG powder, but were small enough to pass through the 0.45  $\mu$ m filter used to prepare the protein solutions. Both spontaneous self-assembly and heat-induced aggregation can be driven by hydrophobic interactions. The correlation between higher VD<sub>3</sub> concentrations and the appearance of more large particles at the expense of  $\beta$ -CG monomers suggests that VD<sub>3</sub> is located within these particles. This is in line with the turbidity data, suggesting that when VD<sub>3</sub> is added dropwise to a  $\beta$ -CG solution, small VD<sub>3</sub>- $\beta$ -CG nanoparticles are formed, which explains the clarification effect; when added to buffer alone, VD<sub>3</sub> aggregated into ~600 nm particles which made the suspension increasingly turbid. When added to  $\beta$ -CG, however, not only did the turbidity remain close to baseline, but no 600 nm peak was observed. This indicates that VD<sub>3</sub> preferentially binds to  $\beta$ -CG, presumably via hydrophobic interactions with lipophilic  $\beta$ -CG patches.

#### UV Absorbance Spectra

Analysis of the UV absorbance spectra provided a qualitative indication of VD<sub>3</sub> binding to  $\beta$ -CG. Figure 5 shows the spectrum of 25  $\mu$ g/ml VD<sub>3</sub> and that of 0.5 mg/ml  $\beta$ -CG individually, as well as that of the mixture of the two solutions (at same final concentrations of the components). As a reference, the spectra of the individual component solutions were summed and plotted. This summation spectrum was then compared to the spectrum of the mixture solution [39,40]. When no interaction occurs, the spectrum of the actual mixture is expected to be indistinguishable from the spectra summation of the individual component solutions. However, the observed deviation from additivity of the two individual spectra provided a strong complementary evidence for  $\beta$ -CG-VD<sub>3</sub> complex formation: The summation spectrum and the complex spectrum were significantly different. Below ~280 nm, the complex had a higher absorbance, and above 280 nm it had

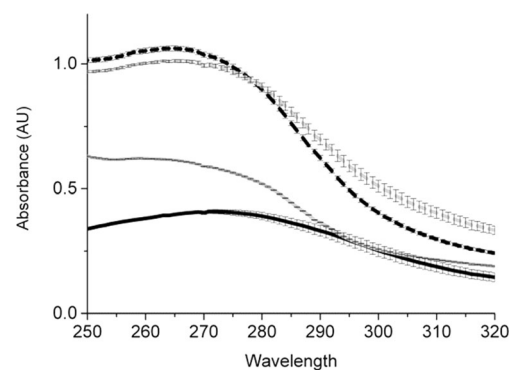


**Fig. 5** Absorbance spectra of 25  $\mu$ g/ml VD (solid black), 0.5 mg/ml  $\beta$ -CG (solid gray),  $\beta$ -CG-VD<sub>3</sub> complex (dashed black) sum of  $\beta$ -CG and VD<sub>3</sub> (dashed gray)

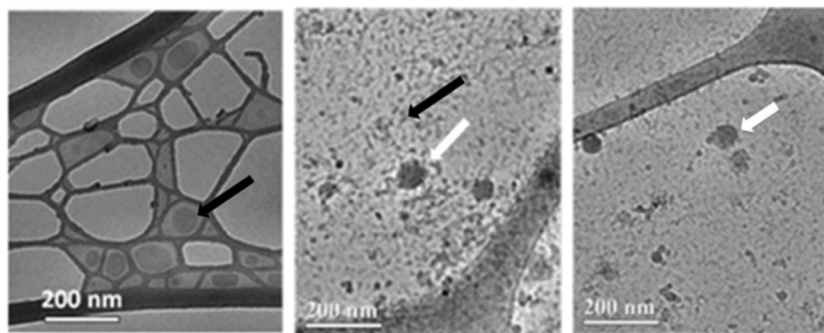


**Fig. 6** Cryo-TEM images (the black grid is the carbon film on which the samples are loaded). Left: 20 µg/ml VD<sub>3</sub> in pH 6.8 PB. Black arrow shows an insoluble VD<sub>3</sub> aggregate; Center: 1 mg/ml β-CG solution. White arrow shows a large (~100 nm diameter) aggregate, black arrow

a lower absorbance than the summation of the components. This suggests that the components of the mixture undergo a physical interaction which changes their inherent absorbance behavior and supports a molecular level association. The somewhat higher absorbance of the mixture compared to the summation, around the peak of VD<sub>3</sub> absorbance (~265 nm [30]), may indicate that the vitamin is in a more hydrophobic environment [41], which is in line with the likely hydrophobic association of the vitamin with the protein. However, additional methods need to be employed for determining the exact mechanism of interaction between the VD<sub>3</sub> and β-CG.

#### Cryo-TEM Microscopy

Cryo-TEM images of VD<sub>3</sub> alone in PB (Fig. 6, left) show that, in the absence of protein, VD<sub>3</sub> aggregates into round droplets. Images of β-CG alone show a few protein aggregates larger than 50 nm (Fig. 6, center, white arrow), while in the background there is an abundance of very small protein particles, most likely corresponding mainly to the soluble β-CG monomers. By comparison, images of VD<sub>3</sub>-β-CG (Fig. 6, right) are similar to images of β-CG alone, also containing a small number of large aggregates, which are most likely VD<sub>3</sub>-β-CG complexes. The VD<sub>3</sub>-β-CG complex particles do not display any morphological characteristics that visually distinguish them from the empty β-CG aggregates in the cryo-TEM images, though the particle size

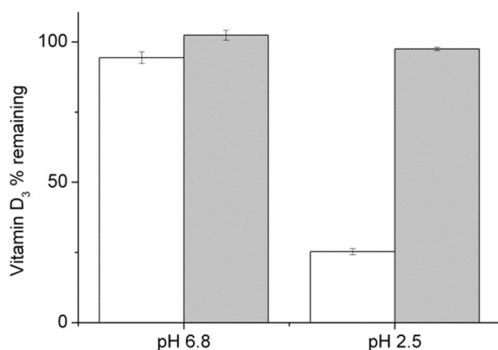


**Fig. 7** Heat Treatment, 30 s at 70 °C. White: VD<sub>3</sub>, Gray: VD<sub>3</sub>-βCG

shows one of the more numerous, small (~10–20 nm diameter) aggregates. Right: White arrow most likely shows a VD<sub>3</sub>-β-CG nanoparticle (VD<sub>3</sub> at 50 µg/ml, 1 mg/ml β-CG)

analysis discussed above (Fig. 3), indicates that the complex solution contains more of these large particles.

#### Thermal Degradation

The aim of the thermal treatment experiment was to determine whether the β-CG protected the vitamin from product

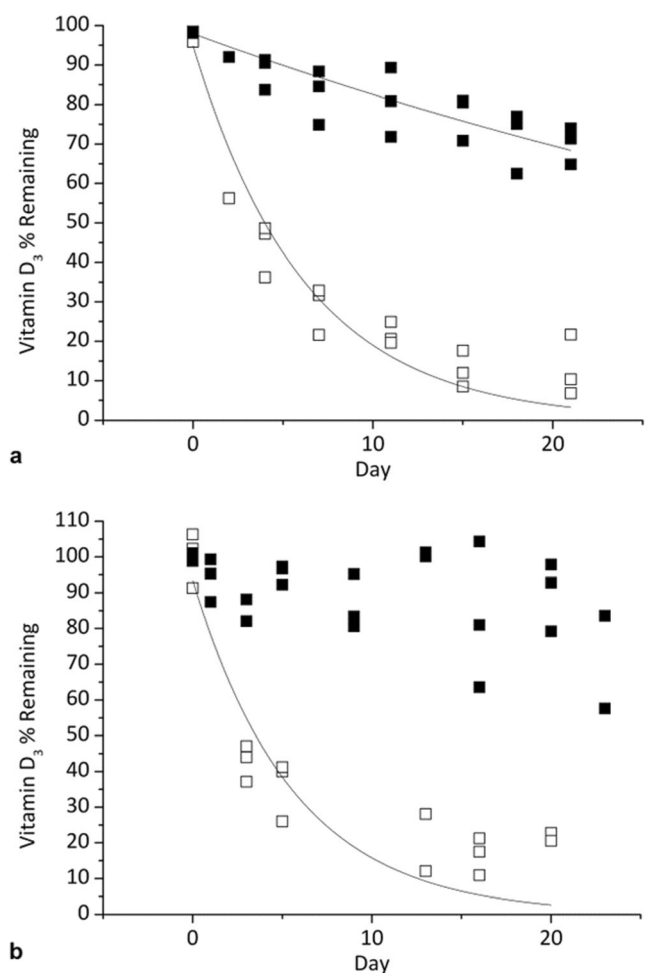


**Fig. 8** Shelf life test at 23 °C, at pH 6.8 (a), pH 2.5 (b). Open: VD<sub>3</sub>, closed: VD<sub>3</sub>-βCG

**Table 1** First-order decay parameters for VD<sub>3</sub> degradation during simulated shelf life

pH		a	Standard Error	k	Standard Error	R <sup>2</sup>
6.8	VD <sub>3</sub>	94.89	4.42	0.161	0.015	0.93
	VD <sub>3</sub> +β-CG	97.95	2.33	0.017	0.002	0.74
2.5	VD <sub>3</sub>	93.45	7.26	0.178	0.031	0.82
	VD <sub>3</sub> +β-CG	–	–	–	–	–

conditions (VD is sensitive to low pH) and processing-related (thermal) degradation. To determine the extent of VD<sub>3</sub> degradation in the heat-treated samples relative to the untreated controls, the integrated peak areas were normalized so that the untreated sample areas were considered 100 %. The heat treatment of 30 s at 70 °C caused no significant (*p* value > 0.05) degradation of both unprotected and protected VD<sub>3</sub> at pH 6.8 (Fig. 7). Indeed, the purpose of such HTST treatments is to produce food products that are free of pathogen contamination, while at the same time leave vitamins and other sensitive components minimally affected by the heat treatment itself. At pH 2.5, however, due to the acid sensitivity of VD, the HTST treatment caused 75 % of the unprotected VD<sub>3</sub> to degrade, while only 2.5 % of the VD<sub>3</sub> in the VD<sub>3</sub>-β-CG nanoparticles were lost. This constituted a significant (*p* < 0.05) degree of protection conferred by the protein to VD<sub>3</sub>.

#### Simulated shelf life test

The results from the two shelf life tests are shown in Fig. 8. In the absence of β-CG, most of the VD<sub>3</sub> degraded within three weeks; 87 % and 70 % of the post-pasteurization VD<sub>3</sub> concentration was lost at pH 6.8 and 2.5, respectively. In contrast, the VD<sub>3</sub>-β-CG nanoparticles retained most of their VD<sub>3</sub> content over the three week period, losing only 30 % and 10 % of the vitamin at pH 6.8 and 2.5, respectively. Thus, β-CG provided excellent protection against VD<sub>3</sub> degradation.

To quantify the difference in encapsulated versus unencapsulated VD<sub>3</sub> degradation rates, we assumed degradation according to first-order kinetics, and used OriginLab<sup>TM</sup> to fit the data using Eq. 2:

$$(2) y = ae^{-kt} \quad (2)$$

In this equation, *y* represents VD<sub>3</sub> concentration after time *t*, *a* represents initial post-pasteurization VD<sub>3</sub> concentration, and *k* represents the decay constant, which has a negative value. The curve fit is presented in Fig. 8, and the values for *a* and *k*, as well as the R<sup>2</sup> values are presented in Table 1. The first-order decay model of unprotected VD<sub>3</sub> at pH 6.8, showed a decay constant, *k*, of 0.161 day<sup>-1</sup>. This is consistent with a reported rate constant for VD<sub>2</sub> oxidation [42]. At the same pH, the VD<sub>3</sub> in the VD<sub>3</sub>-β-CG nanoparticles decayed with an approximately tenfold lower decay constant, *k*=0.017. The unprotected VD<sub>3</sub> fit supports the assumption that the observed degradation follows first order kinetics and, more importantly, that in the presence of β-CG VD<sub>3</sub> degrades at a much lower rate. This protection may be explained by one or a few of several possible mechanisms [2]: β-CG binds to the surface of VD<sub>3</sub> nanoparticles, shielding them from molecular oxygen, free radicals, transition metal ions, and possibly also from incident UV light, thus slowing VD<sub>3</sub> decay. Surprisingly, degradation rate of the unprotected VD<sub>3</sub> at pH 2.5 did not appear to differ dramatically from that at pH 6.8, as evident from the similar decay rate constants of 0.178 vs. 0.161 day<sup>-1</sup> respectively. Also the slow degradation rates of the protected VD<sub>3</sub> were rather similar (although the VD<sub>3</sub>-β-CG data did not fit the first-order model), and the final remaining VD<sub>3</sub> concentration in VD<sub>3</sub>-β-CG pH 2.5 was similar to that at pH 6.8.

#### Simulated Gastric Digestion

Lipophilic molecules such as VD are not readily absorbed in the stomach; instead they are absorbed through the action of micelle-forming bile salts in the small intestine [43]. Therefore, an ideal nanoparticle-based VD<sub>3</sub> delivery system would protect the vitamin from degradation under the extreme acid conditions during gastric digestion. The purpose of this experiment was to evaluate to what extent would β-CG suppress the degradation of VD<sub>3</sub> under proteolytic gastric digestion conditions. As seen in Fig. 9, after two hours of simulated gastric digestion, VD<sub>3</sub>-β-CG nanoparticles retained 92 % of their VD<sub>3</sub> content, while the unprotected VD<sub>3</sub> degraded to 50 % of its starting concentration.

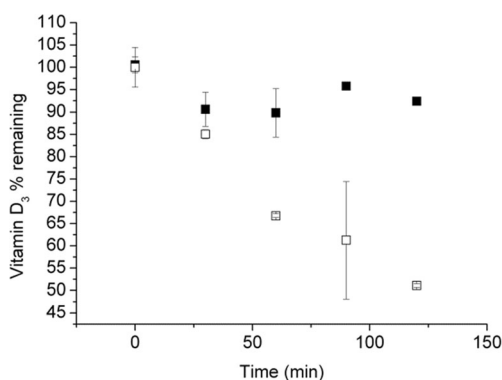


**Fig. 9** VD<sub>3</sub> content during simulated gastric digestion. Open: VD<sub>3</sub>, closed: VD<sub>3</sub>-βCG



The results of the simulated gastric digestion suggest that  $\beta$ -CG is able to retard VD<sub>3</sub> degradation even while simultaneously being digested by a protease. This indicates that the VD<sub>3</sub> remains attached to the peptides resulting from the proteolysis. Thus, although the protein slowly undergoes hydrolysis, the remaining peptides may retain the ability to protect VD<sub>3</sub>. Another possible mechanism of protein protection against VD acid degradation might be related to the buffering capacity of a protein [44], which may provide local protection in its close vicinity.

## Conclusions

VD<sub>3</sub> binds to  $\beta$ -CG, likely via hydrophobic interactions, to form VD<sub>3</sub>- $\beta$ -CG nanoparticles. Formulating VD<sub>3</sub> in these nanoparticles offers several important benefits: nanoparticles are small (50–250 nm) and their solutions are optically clear. Moreover, the entrapment of VD<sub>3</sub> in  $\beta$ -CG nanoparticles provides protection both at pH 6.8 and pH 2.5, and reduces vitamin losses during pasteurization, product shelf life, and gastric digestion.

**Acknowledgments** This study was kindly supported by the Nofar program of the Israeli Ministry of Industry, Trade and Labor, and by Solbar, Plant Extracts (SPE) Ltd.

## References

- M.L. Adams, A. Lavasanifar, G.S. Kwon, *J. Pharm. Sci.* **92**(7), 1343–1355 (2003)
- Y.D. Livney, in *Encapsulation technologies and delivery systems for food ingredients and nutraceuticals*, edited by N. Garti and D. J. McClements (Woodhead Publishing Limited, Oxford, Cambridge, Philadelphia, New Delhi, 2012).
- A. Matalanis, O. Griffith Jones, D.J. McClements, *Food Hydrocoll.* **25**, 1865–1880 (2011)
- E. Semo, E. Kesselman, D. Danino, Y.D. Livney, *Food Hydrocoll.* **21**(5), 936–942 (2007)
- A. Sahu, N. Kasoju, U. Bora, *Biomacromolecules* **9**(10), 2905–2912 (2008)
- P. Zimet, Y.D. Livney, *Food Hydrocoll.* **23**(4), 1120–1126 (2009)
- N. Ron, P. Zimet, J. Bargarum, Y. Livney, *Int. Dairy J.* **20**(10), 686–693 (2010)
- A. Shpigelman, G. Israeli, Y.D. Livney, *Food Hydrocoll.* **24**(8), 735–743 (2010)
- S. Gunasekaran, S. Ko, L. Xiao, *J. Food Eng.* **83**(1), 31–40 (2007)
- L. Liang, M. Subirade, *J. Phys. Chem. B* **114**(19), 6707–6712 (2010)
- S. Avivi, Y. Nitzan, R. Dror, A. Gedanken, *J. Am. Chem. Soc.* **125**(51), 15712–15713 (2003)
- Y.D. Livney, *Curr. Opin. Colloid Interface Sci.* **15**(1–2), 73–83 (2010)
- H. Wang, L. Jiang, L. Fu, *J. Appl. Polym. Sci.* **106**(6), 3716–3720 (2007)
- V.H. Thanh, K. Shibasaki, *J. Agric. Food Chem.* **26**(3), 692–695 (1978)
- J.E. Kinsella, *J. Am. Oil Chem Soc.* **56**(3), 242–258 (1979)
- N. Maruyama, R. Sato, Y. Wada, Y. Matsumura, H. Goto, E. Okuda, S. Nakagawa, S. Utsumi, *J. Agric. Food Chem.* **47**(12), 5278–5284 (1999)
- C.Y. Gan, L.H. Cheng, A.M. Easa, *Innov Food Sci & Emerg Technol.* **9**(4), 563–569 (2008)
- Z. Teng, Y. Luo and Q. Wang, *Journal of Agricultural and Food Chemistry* (2012)
- A. Tapal and P. K. Tiku, *Food Chemistry* (2011)
- Z. Teng, Y. Luo and Q. Wang, *Food Chemistry* (2013)
- S. Utsumi, Y. Matsumura and T. Mori, in *Food Proteins and Their Applications*, ed. by S. Damodaran, A. Paraf (Dekker, New York, 1997), pp. 257–291
- R. Y. Yada, *Proteins in food processing*. (CRC Press, Boca Raton, Fla. [u.a.], 2004).
- K. Tsumura, T. Saito, K. Tsuge, H. Ashida, W. Kugimiya, K. Inouye, *LWT-Food Sci Technol.* **38**(3), 255–261 (2005)
- M.F. Holick, *N. Engl. J. Med.* **357**(3), 266–281 (2007)
- M. Pfeifer, B. Begerow, H. Minne, *Osteoporos. Int.* **13**(3), 187–194 (2002)
- M. Touvier, D.S.M. Chan, R. Lau, D. Aune, R. Vieira, D.C. Greenwood, E. Kampman, E. Riboli, S. Herberg, T. Norat, *Cancer Epidemiol. Biomark. Prev.* **20**(5), 1003 (2011)
- D. Gupta, C. Lammersfeld, K. Trukova, C. Lis, *Prostate Cancer Prostatic Dis.* **12**(3), 215–226 (2009)
- M.F. Holick, *Am. J. Clin. Nutr.* **79**(3), 362–371 (2004)
- T.J. Wang, M.J. Pencina, S.L. Booth, P.F. Jacques, E. Ingelsson, K. Lanier, E.J. Benjamin, R.B. D’Agostino, M. Wolf, R.S. Vasan, *Circulation* **117**(4), 503–511 (2008)
- H.M. Trang, D. Cole, L.A. Rubin, A. Pierratos, S. Siu, R. Vieth, *The Am j of clin nutr.* **68**(4), 854–858 (1998)
- M.S. Calvo, S.J. Whiting, C.N. Barton, *The Am j of clin nutri.* **80**(6), 1710S–1716S (2004)
- T. Loftsson, D. Hreinsdóttir, *AAPS PharmSciTech* **7**(1), 29–32 (2006)
- J.R. Bellare, H.T. Davis, L.E. Scriven, Y. Talmon, *J of Electron Microscop. Technique.* **10**(1), 87–111 (1988)
- M. Haham, S. Ish-Shalom, M. Nodelman, I. Duek, E. Segal, M. Kustanovich, Y.D. Livney, *Food & Function*, 2012
- A. Staffas, A. Nyman, *J. AOAC Int.* **86**(2), 400–406 (2003)
- K. Tsumura, T. Saito, W. Kugimiya, K. Inouye, *J. Food Sci.* **69**(5), C363–C367 (2004)
- S.C. Meredith, M.J. Bolt, I.H. Rosenberg, *J. Colloid Interface Sci.* **99**(1), 244–255 (1984)
- N. Maruyama, M. Adachi, K. Takahashi, K. Yagasaki, M. Kohno, Y. Takenaka, E. Okuda, S. Nakagawa, B. Mikami, S. Utsumi, *Eur. J. Biochem.* **268**(12), 3595–3604 (2001)
- A. Shapira, Y.G. Assaraf, Y.D. Livney, *Nanomed-Nanotechnol.* **6**(1), 119–126 (2010)
- A. Shapira, Y.G. Assaraf, D. Epstein, Y.D. Livney, *Pharm. Res.* **27**, 2175–2186 (2010)
- G. Markman, Y.D. Livney, *Food & Function.* **3**, 262–270 (2012)
- J.M. King, D.B. Min, *J. Am. Oil Chem. Soc.* **79**(10), 983–987 (2002)
- C. P. Coyne, *Comparative Diagnostic Pharmacology: Clinical and Research Applications in Living-System Models*. (Wiley, 2008).
- N.D. Hung, M. Vas, E. Cseke, G. Szabolcsi, *J. Food Sci.* **49**(6), 1535–1542 (1984)